Solid Freeform Fabrication 2022: Proceedings of the 33rd Annual International Solid Freeform Fabrication Symposium – An Additive Manufacturing Conference
Reviewed Paper

EFFECT OF DEFECTS ON THE MECHANICAL PROPERTIES OF LASER POWDER BED FUSED Ti-6Al-4V

Muztahid Muhammad[1,2], Shuai Shao[1,2], Nima Shamsaei[1,2*]

[1] National Center for Additive Manufacturing Excellence (NCAME), Auburn University, Auburn, AL 36849, USA
[2] Department of Mechanical Engineering, Auburn University, Auburn, AL 36849, USA

[*]Corresponding author: shamsaei@auburn.edu
Phone: (334) 844-4839

Abstract

Process-induced volumetric defects are inherent to additively manufactured parts. This study investigates the effect of volumetric defects on the tensile properties of the laser powder bed fused (L-PBF) Ti-6Al-4V specimens fabricated with large variations in process parameters (a total of six sets of process parameters). Cylindrical rods of L-PBF Ti-6Al-4V specimens were stress-relieved before removal from plates and machined to tensile specimens. The defect distribution of specimens resulting from each set of process parameters was analyzed using a high-resolution X-ray computed tomography machine. Quasi-static tensile tests were performed at room temperature using a servo-hydraulic MTS machine. Tensile results were correlated with defect statistics. No apparent difference was observed in the yield strength of the L-PBF Ti-6Al-4V specimens despite the large variations in the process parameters resulting in significant differences in defect content. However, a considerable drop in ductility was observed for the specimens fabricated with insufficient energy.

Keywords: Additive manufacturing, Laser powder bed fusion (L-PBF/LB-PBF), Ti-6Al-4V, Defects, Tensile properties.

Introduction

Additive manufacturing (AM), a layer-wise advance manufacturing technology, has received significant attention as a suitable replacement for conventional subtractive manufacturing methods due to its capability to fabricate parts in near-net-shape conditions with little to no post-processing [1]. The rapid progress of different AM technologies and a better understanding of the process-structure-property relationship of additively manufactured (AM) parts have resulted in increased adoption of AM parts in engineering applications [2,3]. Among different materials that can be fabricated using AM, Ti-6Al-4V is one of the most prominent alloys used in most commercial Ti applications. Conventionally manufactured Ti-6Al-4V components have been widely used in aerospace, automotive, naval, and biomedical sectors [4–6]. The combination of high strength and light weight as well as the ability to sustain in highly corrosive environments and elevated temperatures made Ti-6Al-4V highly desirable in these applications [4,7].

AM method, although it offers numerous benefits over conventional manufacturing methods, AM components often consists of process-induced volumetric defects. The type of defects form in AM parts mainly depend on the fabrication process parameters (e.g., laser power, scan velocity, hatch distance, layer

thickness, etc.). The most common volumetric defects in AM parts are keyhole (KH) pores (usually form due to excessive energy or heat input [8]), lack-of-fusion (LoF) defects (form mostly due to insufficient energy input[9]), and gas-entrapped pores (form due to gas entrapment, supersaturation of metal gas within the melt-pool, etc. [10,11]). In addition, the formation of defects in AM parts may also be affected due to powder characteristics [1,12,13], the volume of parts [14], geometry and location of parts on the build plates [15], etc., even after using recommended process parameters. These process-induced defects can impact the mechanical performance of AM parts [16–18]. It has been reported that the LoF defects, due to their irregular morphology, can cause a significant impact on the tensile properties of laser powder bed fused (L-PBF) Ti-6Al-4V [19–22]. Hence, the impact of defects on the mechanical performance of AM Ti-6Al-4V parts needs to be well understood for the qualification and certification for critical load-bearing applications [23,24].

The formation of volumetric defects and their impact on mechanical properties for AM Ti-6Al-4V parts manufactured via optimized process parameters has been well studied [20,25,34,26–33]. However, based on the studies available in the literature, there is a lack of understanding of how defects type and density impact the tensile properties of L-PBF Ti-6Al-4V. Therefore, this paper investigates the tensile properties of L-PBF Ti-6Al-4V fabricated with large variations in process parameters.

Experimental Procedure

Ti-6Al-4V cylindrical rods were fabricated employing an EOS M290 machine with six different process parameter sets. Apart from the manufacturer recommended process parameter, five other sets of process parameters were used to induce different types of KH and LoF defects. Process parameters (apart from the recommended one) varied so that insufficient or excessive energy induced LoF or KH type defects.The list of the process parameters used in this study is shown in **Table 1**. Following fabrication, the rods were stress-relieved at 705°C for 1 hour with a heating rate of 5°C/minute in an electric furnace and furnace cooled before removing from the build plate. Following stress-relieving, the Ti-6Al-4V rods were machined to round tension test specimens according to the ASTM E8 standard [35] (see **Figure 1**).

Table 1. Process parameters employed for fabricating L-PBF Ti-6Al-4V parts.

Intended defects	Designations	Power, P (W)	Layer thickness (µm)	Scan velocity, V (mm/sec)	Hatch distance, H (µm)	Energy Density, E (J/mm^3)
Recommended	Recom.	280	30	1200	140	55.55
KH	KHa	336		840	140	95.24
KH	KHb	364		960	140	90.28
LoF	LoFa	252		1200	140	50.00
LoF	LoFb	224		1200	140	44.44
LoF	LoFc	280		1200	168	46.29

The defect type and population of specimens fabricated using each process parameter set was analyzed by scanning the middle of the gage section (length of scanned section is ~ 5 mm) employing a Zeiss Xradia 620 Versa X-ray computed tomography (XCT) machine. XCT scanning was performed at 160 KV voltage and 21 W power along with an X-ray filter to reduce the count of low-energy photons.

The voxel size for each scan was kept at ~ 5.5 µm for all conditions. After scanning, the projection images were reconstructed using the Zeiss Xradia software and post-processed using ImageJ software.

Quasi-static tensile tests were conducted using MTS servo-hydraulic testing machine with a load cell capacity of 100 KN according to ASTM E8M standard [35]. Tensile testing was conducted at a strain rate of 0.001 mm/mm/s in displacement-controlled mode. A mechanical extensometer was attached to the specimen to record the strain values till fracture. At least three specimens were tested for each set of process parameters.

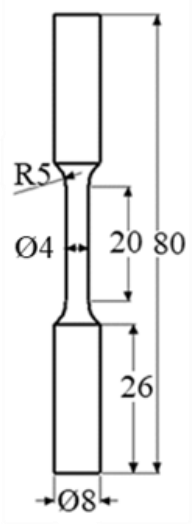

Figure 1. Geometry of the round tension test specimen according to ASTM E8M standard [35]. All the dimensions are in mm.

Results and Discussion

In general, the unique thermal history during fabrication of the AM parts contributes to the formation of process-induced defects (e.g., pores, LoF, etc.). The defect content may increase when thermal energy deviates from the optimized process parameters. Energy density for L-PBF parts can be calculated from the following equation (1) [36]:

$$E = \frac{P}{vht} \quad (1)$$

where E is the energy density, P is the laser power, v is the scanning velocity, h is the hatching distance, and t is the layer thickness.

Typically, excessive thermal energy input results in the formation of KH defects [37]. KH defects form when deep cavities formed due to vapor recoil are “pinched off” at the bottom of the melt pool during solidification [37–39]. On the other hand, LoF defects are irregular in shape and typically form when the insufficient thermal energy density input fails to complete the melting and binding of metallic powders

[28,40,41]. However, regardless of formation types, excessive volumetric defects are undesirable as they can negatively impact mechanical properties [16].

Scanned volumes of L-PBF Ti-6Al-4V specimens fabricated using different process parameters are shown in **Figure 2**. The defect distributions in specimens fabricated using different process parameters are also shown in terms of defect counts per volume and defect volume fraction in **Figure 3**. As seen in **Figure 2** and **Figure 3**, specimens fabricated in manufacturer-recommended process parameters and KHb parameters (i.e., the specimen fabricated using a 30% increase in laser power and 20% decrease in scanning velocity) contained the lowest defect count and density. In addition, the KHa specimen (i.e., the specimen fabricated using a 20% increase in laser power and 30% decrease in scanning velocity, with defect volume fraction of 0.019%) had a slightly increased defect volume fraction (factor of ~6) compared to the recommended (0.003%) and KHb specimens (0.002%). On the other hand, the number of defects and defect volume fraction of LoF specimens are much higher than both recommended and KH specimens (defect volume fraction of LoFa, LoFb, and LoFc specimens are 0.056%, 0.129%, and 0.571%, respectively). It is also observed in **Figure 3**(a) that LoFb and LoFc specimens contained higher number of large defects compared to the recommended, KHa, and KHb specimens. Hence, it is evident that the formation of defects is more sensitive to the reduction of energy input than the increase. Moreover, among LoF specimens, the specimen fabricated with increased hatching distance (i.e., LoFc) consists of the highest defect volume fraction (0.571%), which indicates that increasing hatching distance is more detrimental than decreasing laser power input for L-PBF Ti-6Al-4V specimens.

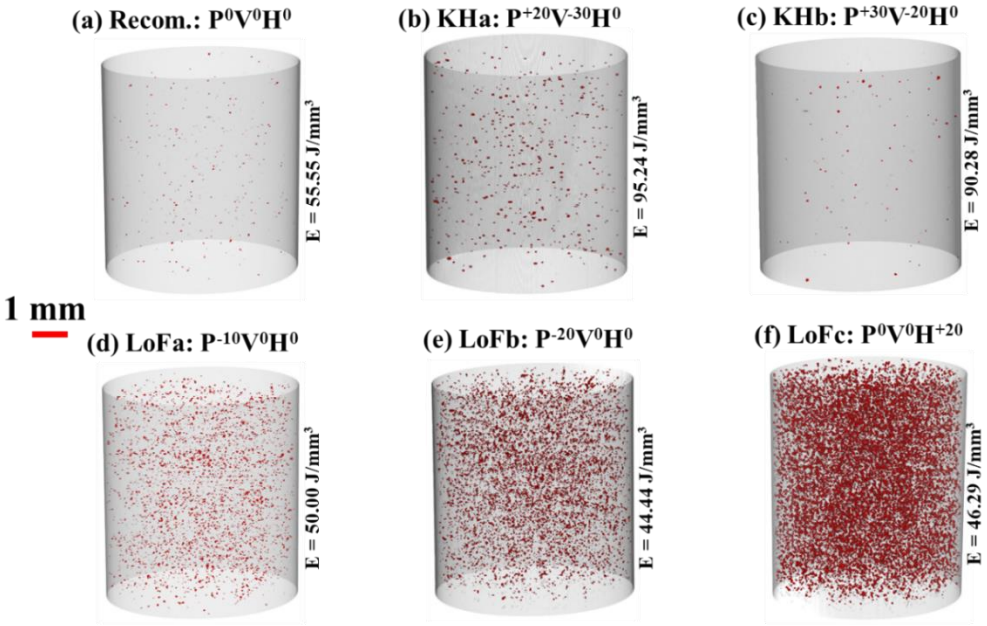

Figure 2. XCT scanned volume of L-PBF Ti-6Al-4V specimens fabricated using different process parameters: (a) Recommended, (b) KHa, (c) KHb, (d) LoFa (e) LoFb, (f) LoFc.

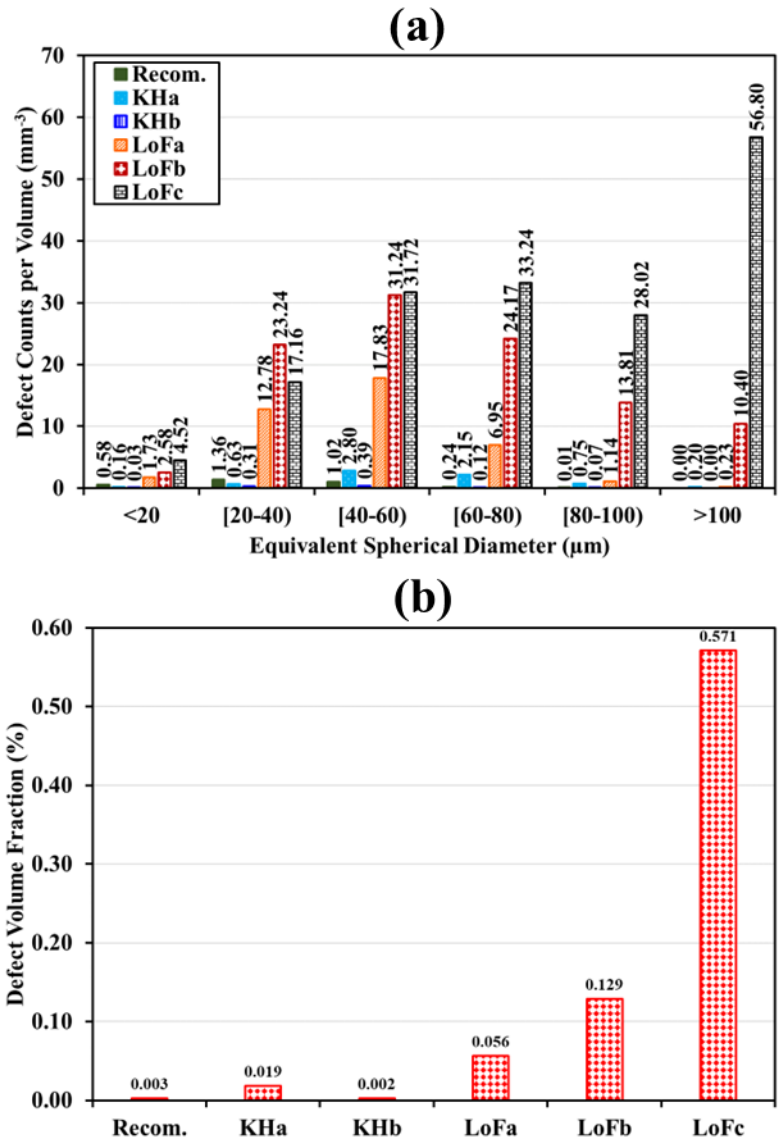

Figure 3. (a) Distribution of defects and (b) percentage of defect volume fraction of L-PBF Ti-6Al-4V specimens fabricated using different process parameters.

The engineering stress-engineering strain curves and column charts presenting tensile properties of L-PBF Ti-6Al-4V specimens fabricated in different process parameters are shown in **Figure 4**. Tensile properties of wrought Ti-6Al-4V annealed at 705°C for 1 hour collected from Metallic Materials Properties Development and Standardization (MMPDS) [42] is also included in **Figure 4**(b) for comparison. Column charts in **Figure 4(b)** include yield strength (S_y), ultimate tensile strength (S_u), and percent elongation to failure (%EL) of the specimens. As seen in **Figure 4**, both KH specimens (i.e., KHa and KHb) exhibit slightly higher tensile strengths (~ 40 MPa higher S_y and S_u compared to the recommended conditions) compared to other conditions. In contrast, all the LoF specimens (i.e., LoFa, LoFb, and LoFc) exhibited comparable tensile strengths (i.e., both S_y and S_u) to the specimens fabricated with recommended parameters. In addition, recommended and KH specimens (both KHa and KHb) showed comparable ductility (i.e., %EL); whereas all the LoF specimens had slightly lower ductility (i.e.,

%EL). All the LoF specimens (i.e., LoFa, LoFb, and LoFc) had similar %EL, ~ 20% lower than recommended and KH ones.

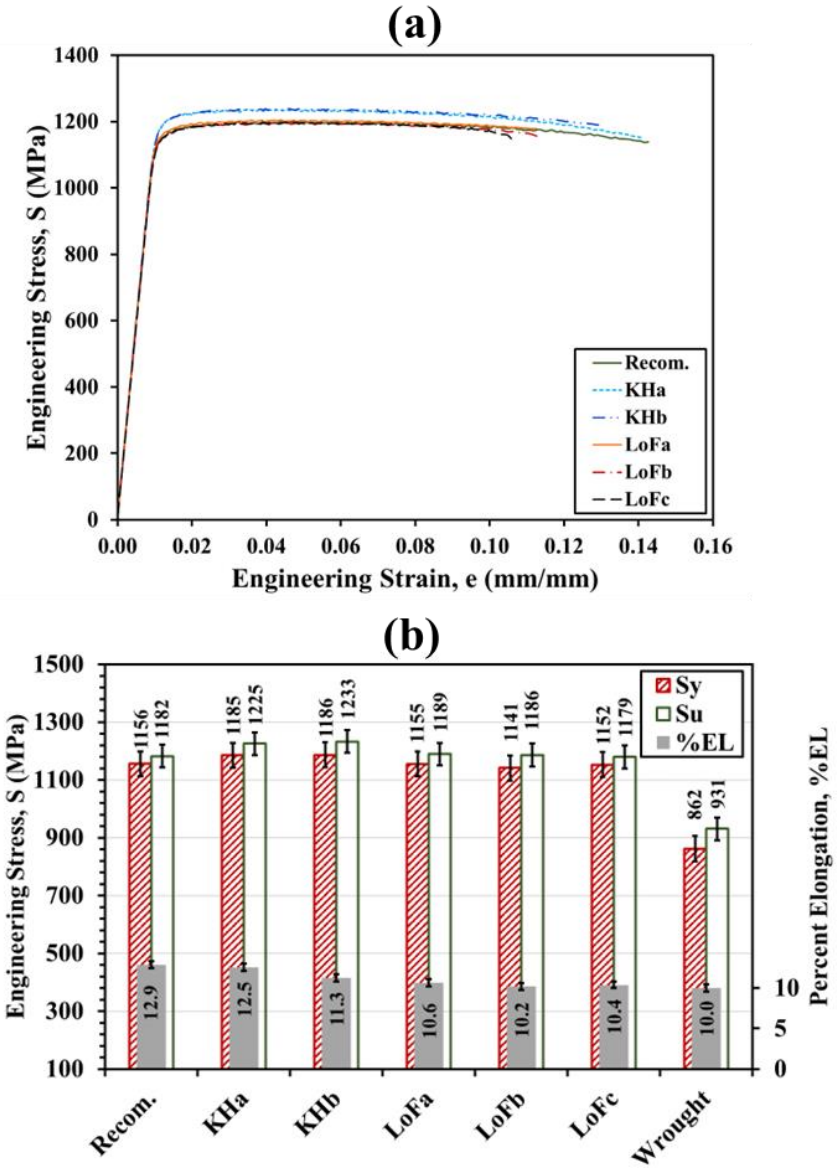

Figure 4. (a) Engineering stress-engineering strain diagram, and (b) column chart comparing tensile properties of L-PBF and wrought (collected from [42]) Ti-6Al-4V specimens fabricated using different process parameters.

Comparable tensile strengths (i.e., both S_y and S_u) of KH specimens compared to the recommended ones can be attributed to the nature of KH defects as well as thermal energy experienced by the KH specimens during the fabrication. It has been reported in the literature that KH defects, even if they form higher in number per volume, do not deteriorate the monotonic properties of AM parts to a significant extent [20]. In addition, excessive laser power can diminish the occurrence of any unmelted/partially melted powder particle in the specimens, thus reducing the possibility of having LoF defects [43]. On the

other hand, LoF specimens in this study were fabricated with 10%-20% less energy density compared to the recommended one resulting in 0.056%-0.571% defect volume fraction in the specimens, which had no apparent effect on the tensile strengths of the L-PBF Ti-6Al-4V specimens. However, the decrease (20%) in ductility (i.e., %EL) in LoF specimens in this study can be attributed to the higher fraction of volumetric defects compared to the recommended one. Volumetric defects acting as crack initiation sites of fracture contributed to the early onset of final fracture compared to the recommended one [20]. Voisin et al. [34] also reported that ductility (i.e., %EL) of AM Ti-6Al-4V is strongly correlated to the defect population present in the specimens. Furthermore, all the L-PBF Ti-6Al-4V studied here exhibited higher tensile strengths (i.e., S_y and S_u) but comparable ductility (i.e., %EL) compared to the wrought T-6Al-4V collected from MMPDS [42]. Based on the above discussion, it is evident that the monotonic test alone is not sufficient for the qualification and certification of AM parts; additional tests (e.g., fatigue) need to be conducted to confirm the quality of AM parts for critical load-bearing applications.

Summary and Conclusions

This study investigated the defect distribution and tensile properties of L-PBF Ti-6Al-4V fabricated using different process parameters. Tensile properties were correlated with defect types and density. The findings of this study can be summarized as follows:

- Upon variation of process parameters, defect distribution of L-PBF Ti-6Al-4V changed. Insufficient energy density resulted in more defect contents than excessive energy density during the fabrication.
- L-PBF Ti-6Al-4V specimens even fabricated with defects using non-optimized process parameters exhibited comparable tensile strength to the recommended one.
- Defects in Ti-6Al-4V specimens negatively impacted the ductility compared to the recommended one, contributing to the early onset of the final fracture.

Acknowledgment

The authors greatly acknowledge the support provided by the Federal Aviation Administration (FAA) under Cooperative Agreement 12-C-AM-AU and the National Science Foundation (NSF) under grant # 1919818.

References

[1] J.W. Pegues, S. Shao, N. Shamsaei, N. Sanaei, A. Fatemi, D.H. Warner, P. Li, N. Phan, Fatigue of additive manufactured Ti-6Al-4V, Part I: The effects of powder feedstock, manufacturing, and post-process conditions on the resulting microstructure and defects, Int. J. Fatigue. 132 (2020) 105358.

[2] T. DebRoy, T. Mukherjee, J.O. Milewski, J.W. Elmer, B. Ribic, J.J. Blecher, W. Zhang, Scientific, technological and economic issues in metal printing and their solutions, Nat. Mater. 18 (2019) 1026–1032.

[3] T. Wohlers, N. Mostow, I. Campbell, O. Diegel, J. Kowen, I. Fidan, Wohlers Report 2022, (2022) 427.

[4] C. Leyens, M. Peters, Titanium and Titanium Alloys, Wiley, 2003.

[5] B. Vamsi Krishna, W. Xue, S. Bose, A. Bandyopadhyay, Engineered porous metals for implants, JOM. 60 (2008) 45–48.
[6] M. Niinomi, Mechanical biocompatibilities of titanium alloys for biomedical applications, J. Mech. Behav. Biomed. Mater. 1 (2008) 30–42.
[7] R.R. Boyer, An overview on the use of titanium in the aerospace industry, Mater. Sci. Eng. A. 213 (1996) 103–114.
[8] W.E. King, H.D. Barth, V.M. Castillo, G.F. Gallegos, J.W. Gibbs, D.E. Hahn, C. Kamath, A.M. Rubenchik, Observation of keyhole-mode laser melting in laser powder-bed fusion additive manufacturing, J. Mater. Process. Technol. 214 (2014) 2915–2925.
[9] H. Gong, K. Rafi, H. Gu, T. Starr, B. Stucker, Analysis of defect generation in Ti–6Al–4V parts made using powder bed fusion additive manufacturing processes, Addit. Manuf. 1–4 (2014) 87–98.
[10] W.J. Sames, F.A. List, S. Pannala, R.R. Dehoff, S.S. Babu, The metallurgy and processing science of metal additive manufacturing, Int. Mater. Rev. 61 (2016) 315–360.
[11] M.C. Brennan, J.S. Keist, T.A. Palmer, Defects in Metal Additive Manufacturing Processes, J. Mater. Eng. Perform. 30 (2021) 4808–4818.
[12] A. du Plessis, S.G. le Roux, Standardized X-ray tomography testing of additively manufactured parts: A round robin test, Addit. Manuf. 24 (2018) 125–136.
[13] A. Poudel, A. Soltani-Tehrani, S. Shao, N. Shamsaei, Effect of powder characteristics on tensile properties of additively manufactured 17-4 PH stainless steel, Proc. 32nd Solid Free. Fabr. Symp. (2021) 870-878.
[14] R. Shrestha, J. Simsiriwong, N. Shamsaei, Fatigue behavior of additive manufactured 316L stainless steel under axial versus rotating-bending loading: Synergistic effects of stress gradient, surface roughness, and volumetric defects, Int. J. Fatigue. 144 (2021) 106063.
[15] W. Xu, M. Brandt, S. Sun, J. Elambasseril, Q. Liu, K. Latham, K. Xia, M. Qian, Additive manufacturing of strong and ductile Ti–6Al–4V by selective laser melting via in situ martensite decomposition, Acta Mater. 85 (2015) 74–84.
[16] M. Muhammad, P.D. Nezhadfar, S. Thompson, A. Saharan, N. Phan, N. Shamsaei, A comparative investigation on the microstructure and mechanical properties of additively manufactured aluminum alloys, Int. J. Fatigue. 146 (2021) 106165.
[17] M.S. Dodaran, M. Muhammad, N. Shamsaei, S. Shao, Synergistic effect of microstructure and defects on the initiation of fatigue cracks in additively manufactured Inconel 718, Int. J. Fatigue. 162 (2022) 107002.
[18] A. Poudel, N. Shamsaei, S. Shao, Linear elastic finite element calculations of short cracks initiated from the defects: effect of defect shape and size, Proc. 32nd Solid Free. Fabr. Symp. (2021) 915-922.
[19] A. du Plessis, I. Yadroitsava, I. Yadroitsev, Effects of defects on mechanical properties in metal additive manufacturing: A review focusing on X-ray tomography insights, Mater. Des. 187 (2020) 108385.
[20] T. Montalbano, B.N. Briggs, J.L. Waterman, S. Nimer, C. Peitsch, J. Sopcisak, D. Trigg, S. Storck, Uncovering the coupled impact of defect morphology and microstructure on the tensile behavior of Ti-6Al-4V fabricated via laser powder bed fusion, J. Mater. Process. Technol. 294 (2021) 117113.
[21] A. Soltani-Tehrani, M.S. Yasin, S. Shao, M. Haghshenas, N. Shamsaei, Effects of Powder Particle Size on Fatigue Performance of Laser Powder-Bed Fused Ti-6Al-4V, Procedia Struct. Integr. 38 (2022) 84–93.

[22] A. Soltani-Tehrani, M.S. Yasin, S. Shao, N. Shamsaei, Effects of Stripe Width on the Porosity and Mechanical Performance of Additively Manufactured Ti-6Al-4V Parts, Proc. 32nd Solid Free. Fabr. Symp. (2021) 1061–1075.
[23] M. Seifi, M. Gorelik, J. Waller, N. Hrabe, N. Shamsaei, S. Daniewicz, J.J. Lewandowski, Progress Towards Metal Additive Manufacturing Standardization to Support Qualification and Certification, JOM. 69 (2017) 439–455.
[24] R. Russell, D. Wells, J. Waller, B. Poorganji, E. Ott, T. Nakagawa, H. Sandoval, N. Shamsaei, M. Seifi, Qualification and certification of metal additive manufactured hardware for aerospace applications, Addit. Manuf. Aerosp. Ind. (2019) 33–66.
[25] S. Lee, N. Ahmad, K. Corriveau, C. Himel, D.F. Silva, N. Shamsaei, Bending properties of additively manufactured commercially pure titanium (CPTi) limited contact dynamic compression plate (LC-DCP) constructs: Effect of surface treatment, J. Mech. Behav. Biomed. Mater. 126 (2022) 105042.
[26] P. Wang, M.H. Goh, Q. Li, M.L.S. Nai, J. Wei, Effect of defects and specimen size with rectangular cross-section on the tensile properties of additively manufactured components, Virtual Phys. Prototyp. 15 (2020) 251–264.
[27] X.-Y. Zhang, G. Fang, S. Leeflang, A.J. Böttger, A. A. Zadpoor, J. Zhou, Effect of subtransus heat treatment on the microstructure and mechanical properties of additively manufactured Ti-6Al-4V alloy, J. Alloys Compd. 735 (2018) 1562–1575.
[28] G. Kasperovich, J. Haubrich, J. Gussone, G. Requena, Correlation between porosity and processing parameters in TiAl6V4 produced by selective laser melting, Mater. Des. 105 (2016) 160–170.
[29] R. Laquai, B.R. Müller, G. Kasperovich, G. Requena, J. Haubrich, G. Bruno, Classification of Defect Types in SLM Ti-6Al-V4 by X-ray Refraction Topography, Mater. Perform. Charact. 9 (2020) 20190080.
[30] M. Tang, P.C. Pistorius, J.L. Beuth, Prediction of lack-of-fusion porosity for powder bed fusion, Addit. Manuf. 14 (2017) 39–48.
[31] R. Cunningham, S.P. Narra, T. Ozturk, J. Beuth, A.D. Rollett, Evaluating the Effect of Processing Parameters on Porosity in Electron Beam Melted Ti-6Al-4V via Synchrotron X-ray Microtomography, JOM. 68 (2016) 765–771.
[32] M. Muhammad, M. Masoomi, B. Torries, N. Shamsaei, M. Haghshenas, Depth-sensing time-dependent response of additively manufactured Ti-6Al-4V alloy, Addit. Manuf. 24 (2018) 37–46.
[33] M. Muhammad, J.W. Pegues, N. Shamsaei, M. Haghshenas, Effect of heat treatments on microstructure/small-scale properties of additive manufactured Ti-6Al-4V, Int. J. Adv. Manuf. Technol. 103 (2019) 4161–4172.
[34] T. Voisin, N.P. Calta, S.A. Khairallah, J.-B. Forien, L. Balogh, R.W. Cunningham, A.D. Rollett, Y.M. Wang, Defects-dictated tensile properties of selective laser melted Ti-6Al-4V, Mater. Des. 158 (2018) 113–126.
[35] ASTM E8, ASTM E8/E8M standard test methods for tension testing of metallic materials 1, Annu. B. ASTM Stand. 4. (2010) 1–27.
[36] L. Thijs, F. Verhaeghe, T. Craeghs, J. Van Humbeeck, J.-P. Kruth, A study of the microstructural evolution during selective laser melting of Ti–6Al–4V, Acta Mater. 58 (2010) 3303–3312.
[37] W.E. King, H.D. Barth, V.M. Castillo, G.F. Gallegos, J.W. Gibbs, D.E. Hahn, C. Kamath, A.M. Rubenchik, Observation of keyhole-mode laser melting in laser powder-bed fusion additive manufacturing, J. Mater. Process. Technol. 214 (2014) 2915–2925.
[38] L. Wang, Y. Zhang, H.Y. Chia, W. Yan, Mechanism of keyhole pore formation in metal additive

manufacturing, Npj Comput. Mater. 8 (2022) 22.
[39] A.M. Kiss, A.Y. Fong, N.P. Calta, V. Thampy, A.A. Martin, P.J. Depond, J. Wang, M.J. Matthews, R.T. Ott, C.J. Tassone, K.H. Stone, M.J. Kramer, A. van Buuren, M.F. Toney, J. Nelson Weker, Laser-Induced Keyhole Defect Dynamics during Metal Additive Manufacturing, Adv. Eng. Mater. 21 (2019) 1900455.
[40] A. Soltani-Tehrani, R. Shrestha, N. Phan, M. Seifi, N. Shamsaei, Establishing specimen property to part performance relationships for laser beam powder bed fusion additive manufacturing, Int. J. Fatigue. 151 (2021) 106384.
[41] R. Shrestha, N. Shamsaei, M. Seifi, N. Phan, An investigation into specimen property to part performance relationships for laser beam powder bed fusion additive manufacturing, Addit. Manuf. 29 (2019) 100807.
[42] R.C. Rice, J.L. Jackson, J. Bakuckas, S. Thompson, Metallic Materials Properties Development and Standardization (MMPDS). | National Technical Reports Library - NTIS, (2003) 1728.
[43] A. Soltani-Tehrani, M. Habibnejad-Korayem, S. Shao, M. Haghshenas, N. Shamsaei, Ti-6Al-4V powder characteristics in laser powder bed fusion: The effect on tensile and fatigue behavior, Addit. Manuf. 51 (2022) 102584.